Molecular architectural changes in hydrated macroporous styrene–divinylbenzene resin sorbents revealed by transmission electron microscopy using image analysis

I. M. Huxham, B. Rowatt and D. C. Sherrington*
Department of Pure and Applied Chemistry, University of Strathclyde, Glasgow G1 1XL, UK

and L. Tetley
EM Biological Laboratory, Chemistry Building, University of Glasgow, Glasgow G12 8QQ, UK
(Received 19 February 1991; revised 26 August 1991; accepted 1 October 1991)

A range of hydrophobic sorbent polymers based on crosslinked polystyrene have been prepared with high nominal crosslink ratios of 55–100%, and with varying levels of toluene as a porogen (comonomer/porogen volume ratios of 0.5/1, 1/1, 2/1 and 3/1). Contrast enhanced, energy filtered transmission electron micrographs, from dry and freeze-dried polymer embedded in Lowicryl resin and from frozen-hydrated sections of these sorbents, have been obtained in order to allow a direct visual comparison of these materials to be made without using heavy metal stains. In addition, 'real-time' electron microscopical images were captured via a video output to generate segmented pixel arrays in which grey level values were used to produce quantitative data relating to the polymers' pore structure. This was achieved by applying unsophisticated computer-assisted image analysis techniques. Despite the hydrophobic character of the sorbents, the results show clearly that these matrices expand significantly on hydration and that major changes in the pore sizes and their distribution take place. The relative changes observed within the matrix of sorbents examined are discussed in terms of the currently accepted structural models of pore structure. The techniques described offer the prospect of characterizing polymer sorbents in their hydrated and therefore applied state, and hence lay the foundation for a more rational design of sorbents in the future.

(Keywords: styrene–divinylbenzene sorbents; electron microscopy; hydrated polymeric sorbents; image analysis)

INTRODUCTION

Styrene–divinylbenzene resins form the basis of a wide range of commercially available ion-exchange resins, in which sulphonate groups are introduced to allow the exchange of cations, or quaternary ammonium groups to allow the exchange of anions[1]. Increasingly, however, non-functional resins are being employed as hydrophobic sorbents[2], useful on the one hand for removing toxic contaminants (e.g. phenols) from river, ground or waste water[3], and on the other hand, for recovering, under very mild conditions, sensitive bioorganic molecules (e.g. cephalosporin C) from production fermentation broths[4,5]. The current understanding of the molecular structure and morphology of such sorbents is perhaps best presented in recent seminal reviews by Albright[6] and Guyot[7].

The design and optimization of sorbents for the recovery of bioorganics have been achieved essentially by a trial and error process, and there is still a dearth of understanding in the correlation of sorbent structure (and sorbent synthesis procedure) with sorbent performance. We have recently completed a fundamental study in this area, upon which we shall shortly report[8]. In the course of this work we have also carried out a very detailed transmission electron microscopy (TEM) study of sorbents prepared in-house, with the objective of quantifying the pore structure of sorbents both in the 'dry' and the 'wet' state. Transmission electron micrographs of 'dry' resins have been published before[6,9] but to our knowledge there has never been any attempt by other researchers to image 'wet' macroporous polystyrenes, nor to subject the resultant micrographs to intense image analysis procedures. While porosity data (e.g. N_2 sorption/desorption; Hg intrusion porosimetry) for 'dry' samples are readily obtained and can be very useful in formulating an understanding of sorbent structure and performance, there has always been an underlying worry that such data refer to sorbents in a physical state far removed from that which actually prevails during use.

Recently there have been very significant advances in the application of computer assisted analysis of video grey level data[10] (grey values from 0 to 225 for each pixel) and it is very attractive to couple a transmission electron microscope to a video output and computer support. This allows data from several live images of sectioned material to be pooled and hence to generate

*To whom correspondence should be addressed

0032-3861/92/132768-10

morphometric measurements from the sample with some degree of accuracy. Spatially resolved details of matrices can be obtained following the generation of parameters which describe the area, diameter, perimeter length, shape and circularity of the observed pore structure. We have already presented a preliminary report on our application of these techniques to polymer resin sorbents[11] and now describe the detailed results for a specific matrix of polymeric sorbents.

Very significant advances have also been made in the cryomanipulation of samples for TEM, driven by the requirement to protect and retain the morphology of hydrated biological samples during imaging[12,13]. To our knowledge such techniques have not been applied to resin sorbents outside this laboratory and this paper also reports on our successful use of these procedures in producing images of hydrated sorbents. Such images have also been subjected to computer grey level analysis, to allow quantitative comparison with 'dry' resins to be made.

EXPERIMENTAL

Materials

Commercial divinylbenzene (Aldrich, ~55 vol% *m*- and *p*-divinylbenzenes; ~45 vol% *m*- and *p*-ethylstyrenes); special grade divinylbenzene (Dow, ~80 vol% *m*- and *p*-divinylbenzenes; ~20 vol% *m*- and *p*-ethylstyrenes); toluene (May and Baker, analytical grade) and 2-ethylhexan-1-ol (BDH, general purpose reagent) were all used as supplied.

Preparation of p-divinylbenzene

Sodium hydride (80% dispersion in oil, 18.0 g) in a 2 l three-necked flask was washed three times with sodium dried ether to remove the oil. The flask was stoppered and fitted with a magnetic stirrer. Nitrogen gas was passed through the flask for the duration of the reaction. Dimethylsulphoxide (DMSO, 200 ml) was added to the flask and the mixture was heated to 75–80°C for 45 min. The resulting solution was cooled in an ice–water bath and methyltriphenyl phosphonium bromide (214.2 g) in DMSO (400 ml) was added. The solution of the ylide formed was then stirred for 10 min before use. Terephthaldicarboxaldehyde (33.6 g) in DMSO (200 ml) was added, and stirring was continued for 3 h at room temperature and 1.5 h at 60°C. After this time the reaction mixture was cooled and poured into 500 ml of cold water. The mixture was filtered to remove the precipitate that had formed. The solution was shaken with five 200 ml fractions of n-pentane. The organic fractions were combined, washed with water, and dried over anhydrous sodium sulphate. The pentane was removed on a rotary evaporator to give the product (yield = 29.4; 90%). ^{1}H n.m.r. 250 MHz ($CDCl_3$); δ = 5.1–5.9 (2d, 2p, $=CH_2$); 6.5–6.9 (d, 1p, $-CH=$); 7.35 (m, 4p, aromatic).

Preparation of polymer sorbents

Sorbents were prepared by a conventional free-radical suspension polymerization procedure using a technique reported already[14]. In this instance, however, the scale of each reaction was reduced such that typically ~4 g of resin was obtained each time. This allowed for the efficient utilization of the pure *p*-divinylbenzene prepared in-house. Yields of beaded product were always >90%, and samples were freed of porogens and any residual monomer by exhaustive extraction with acetone before drying under vacuum (40°C, 24 h). Typically particle sizes were in the range 250–1000 μm and representative samples were always selected for TEM analysis.

Polymers suitable for sorbent application generally have a minimum requirement of a high surface area and these can be synthesised by use of relatively high levels of divinylbenzene, together with a solvating porogen, e.g. toluene. *Table 1* shows the constituent mixtures used to prepare the matrix of sorbents in this work, and for comparison a sorbent prepared with a precipitating porogen, 2-ethyl-hexanol, has been included.

Specimen preparation

A representative sample of each sorbent (250–1000 μm diameter, ~50 individual beads) was washed with methanol then vacuum dried (60°C, 24 h). These constituted the 'dry' sorbents for analysis.

A second similar sample of each sorbent was first wetted with methanol and then washed with increasing proportions of water/methanol mixtures, and finally incubated overnight at 4°C in doubly distilled water. For cryopreservation a single layer of hydrated beads (~10 individuals) was spread onto a small aluminium pin for ease of handling, and to maximize contact with the cryogen. The excess water was carefully removed with filter paper and the beads were then mixed with an equal volume of Tissue-Tek (OCT compound, Miles, USA) to ensure that they did not become detached from the pin during drying. The pin was plunge-frozen in a mixture of liquid propane/isopentane at −160°C within a Reichert KF80 device, and then transferred into a Balzers freeze-drying unit at −150°C. The amorphous ice within the sorbent was removed at −70°C by slow freeze-drying (overnight) in vacuum at 1.33×10^{-4} Pa, and brought to room temperature at a rate of 10°C h^{-1}. These constituted the 'freeze-dried' sorbents for analysis.

Both dry and freeze-dried beads were placed into Lowicryl resin K4M (a hydrophilic methacrylate resin containing 4.8% crosslinker; Chemische Werke Lowi,

Table 1 Composition of polymerization mixtures used to prepare resin sorbents

Sorbent	Divinyl benzene[a] (vol%)	*m*-, *p*-ethyl vinylbenzene (vol%)	Volume ratio porogen[b] to comonomers
PS55X0.7T	*p*-, *m*-; 55	45	0.5
1T			1
2T			2
3T			3
PS80X0.5T	*p*-, *m*-; 80	20	0.5
1T			1
2T			2
3T			3
PS100X0.5T	*p*-; 100	0	0.5
1T			1
2T			2
3T			3
PS20X1ET	*p*-, *m*-; 20	16[c]	1[d]

[a]See Experimental for details
[b]Toluene
[c]Remainder, styrene 64 vol%
[d]2-Ethylhexanol

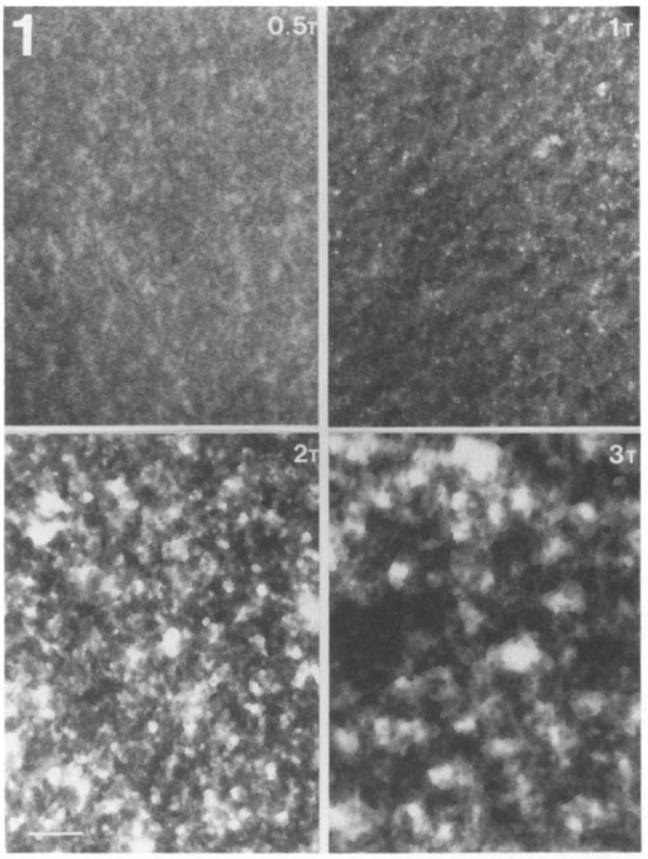

Figure 1 Transmission electron micrographs of dry samples of sorbents PS55X0.5T, 1T, 2T and 3T. Bar = 250 nm

Germany). Penetration of the embedding resin into the sorbent bead structure was facilitated using a vacuum. The resin was cured according to the manufacturer's recommendations using u.v. light for 2 days. Embedding in such a resin aids retention of the fine structural detail of the sample matrix during thin sectioning. In biological samples this process is not believed to induce any significant structural changes but it is not known to what extent the precured embedding resin might solvate polystyrene. Since both groups of sorbents (dry and freeze-dried) were treated similarly, however, any influence would be expected to be common to both groups of samples. Sections of each embedded sorbent were cut at a nominal thickness of ~70 nm on a Reichert Ultracut E microtome using a glass or diamond knife. They were then mounted onto uncoated grids ready for TEM analysis. Each section contained a cross-sectional element from one bead.

A third (selected) group of sorbents were each hydrated and plunge-frozen at −160°C as described above. Each was then sectioned at −50°C (embedded only in its own amorphous ice) within the ultra-cryomicrotome using a nominal thickness of 80 nm and a pentanol-filled glass knife[10,15]. Sections were mounted on 700 hexagonal mesh copper grids to provide the maximum support for fragile samples, and then analysed as outlined below.

Electron microscopy and image analysis

The above mounted samples were observed unstained using enhanced contrast on a Zeiss 902 electron microscope at 80 kV. With the exception of the outer ~500 nm shell of each bead, the polymer structure was consistent throughout. Micrographs for photography were taken at 50 000 × magnification (*Figures 1–3* show dry samples PS55X, PS80X, PS100X, respectively), and images for pore structure analysis were collected at 20 000 × by insertion of a fluorescent screen at 45° to the beam, and detecting the emitted light using a Cohu CCD video camera. For each sample an area of 1 μm^2 was observed within the main body of a bead cross-section. Magnification at this level allowed direct comparisons of all polymers to be made without a significant loss in resolution; the minimum measurable pore diameter was 3 nm.

Live images were collected using a constant beam brightness in which both the spot size and contrast aperture diameter remained fixed to ensure identical contrast and beam intensity for each specimen. These settings resulted in pores within the polymer network (filled with Lowicryl resin in the dry and freeze-dried samples) gaining grey level values of 255 (where 0 is black and 255 is white). Image analysis was carried out using the Sight Systems Freelance package (version 5.20) with integral image manager, which resolved a 512 × 512 pixel area into 256 grey levels. A grey level threshold of 180/255 was set prior to capture of 10 or 20 images of an area 1 μm^2 from at least two different beads for each sorbent. The lower grey level value (180) defines the pore profile boundary and was chosen in conjunction with the electron beam intensity to comply with the resolution limits (3 nm) of the microscope, the video camera and the computer at this magnification. Live images (grey level ranges 45–255) were shade corrected to accommodate the inherent centre bias of the video camera system and used to generate binary images of the pore profiles[15].

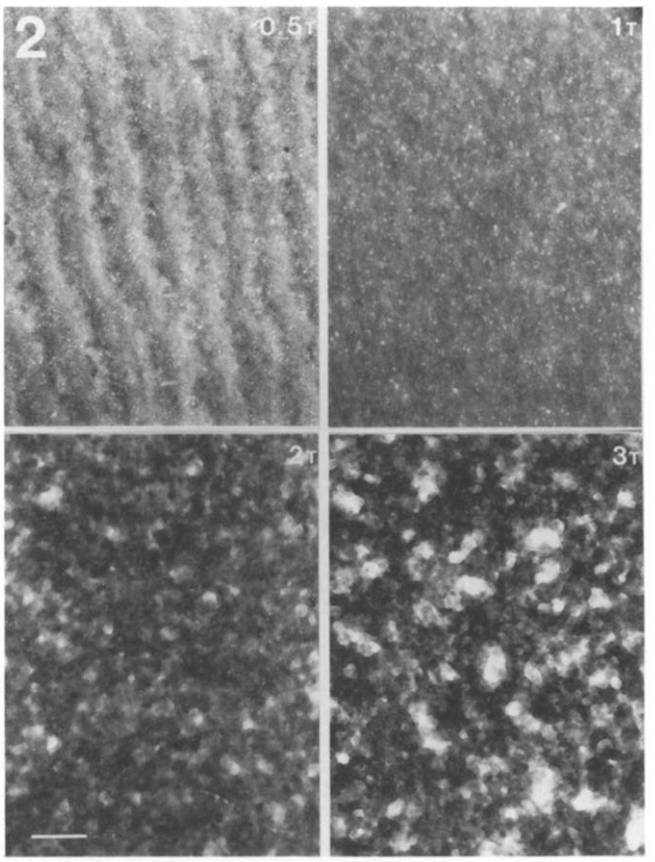

Figure 2 Transmission electron micrographs of dry samples of sorbents PS80X0.5T, 1T, 2T and 3T. Bar = 250 nm

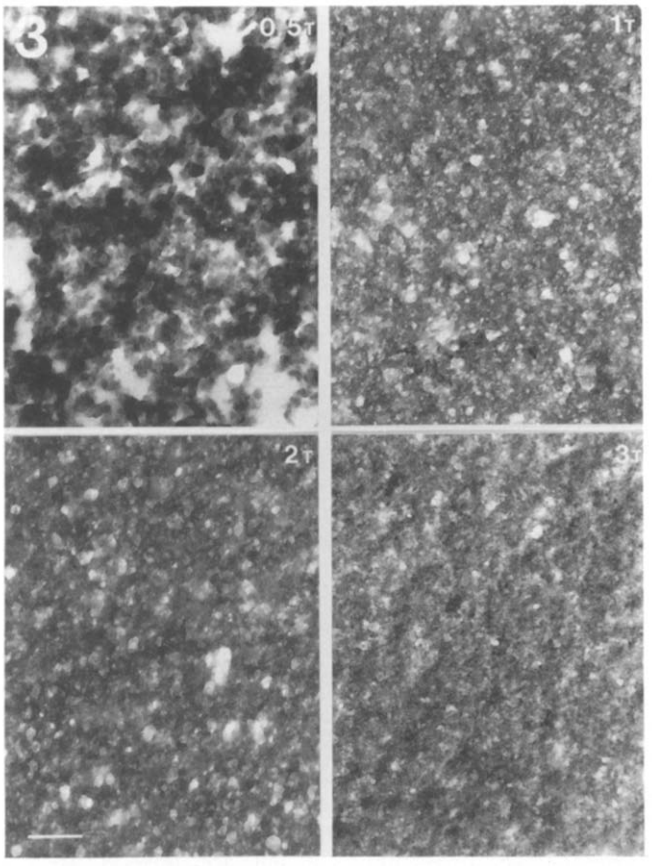

Figure 3 Transmission electron micrographs of dry samples of sorbents PS100X0.5T, 1T, 2T and 3T. Bar = 250 nm

Measurement and data analysis

Binary images were used to produce parameters of pore cross-sectional area, A, pore perimeter, p, the maximum pore diameter, d, and width, w, of each pore profile within the area of analysis, calibrated in nanometres (*Figure 4*). Data derived from two or more different polymer beads were pooled by cumulatively appending data from each binary image into one data file prior to analysis. These data were used to calculate the total pore cross-sectional area, average pore profile diameter, the area as a percentage of the total area representative of pores within a specific range of pore diameters, average pore profile circularity and average pore profile shape. Area simply counts the number of pixels within and including the pore profile boundary. Perimeter is a more complex measurement based on a smoothed version of the outer edge of the pore profile. Maximum diameter calculates the longest chord in the pore profile by first calculating the pore profile centroid and then determining the further point until the process converges. Width is the projection of the pore profile onto an axis perpendicular to the longest chord. Circularity is defined by $4\pi A/p^2$, where unity is a circle, and shape by A/dw, where the lower the value the greater the distortion of shape. The latter two parameters determine changes which are not necessarily detected by simple measurements of pore profile area and diameter. All data showed significant ranges and so are quoted as averages.

It is perhaps worth emphasizing that since this technique quantifies thin pore sections, the pore cross-sectional area parameter, A, should correlate most closely with conventionally determined pore volume data; the pore perimeter parameter, p, with conventionally determined pore surface area, and the pore diameter, d, with conventional pore diameter. We have established such a correlation and will be presenting the results in a separate paper[16].

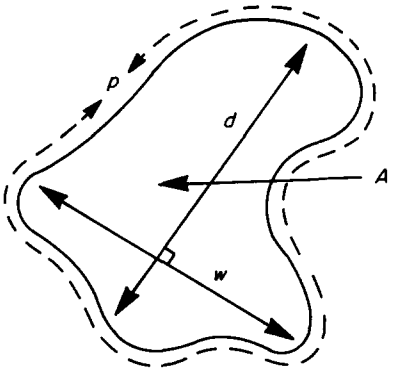

Figure 4 Styrene–divinylbenzene resin sorbent pore profile parameters: A = pore profile cross-sectional area; d = maximum pore profile diameter; w = pore profile width; p = pore profile perimeter; pore profile circularity = $4\pi A/p^2$; pore profile shape = A/dw

RESULTS AND DISCUSSION

Limitations to the use of image analysis

Sectioning of frozen hydrated material inevitably causes some damage to the sample, but such artefactual damage is always difficult to assess. Solvation of the section on the grid by residual pentanol or severe structural deformation of the polymer during sectioning of hydrated material (particularly on 'dry' knives, data not shown), are both likely to affect significantly any subsequent analysis of the image. In this respect analysis of freeze-dried, resin embedded material is less likely to be subject to this sort of effect and is therefore likely to provide a more consistent hydrodynamic structure for analysis (see below). Micrographs of PS20X1ET, PS55X1T and PS100X1T in their dry, freeze-dried and frozen forms are shown in *Figures 5–7*.

An analytical sequence based upon grey level values for a pixel array representing an image is very dependent upon the adoption of consistent methods. Image contrast can be affected by variations in section thickness, spot size, beam intensity, contrast aperture setting, by differential staining and from selective beam damage. Thus it is important to ensure that each setting of the microscope, video camera and computer system is maintained from one image to the next. The Zeiss 902 EM is particularly useful in this respect since elimination of the inelastically scattered electrons, via insertion of a 20 eV window into the beam before imaging, markedly improves the contrast of unstained material to produce an image which can be related directly to polymer mass. Choosing a threshold value from the grey level image to generate a binary image will determine the limits of the pore profile outline and the magnification will determine the level of resolution[15]. In both cases, however, the relative density will nevertheless represent a clear pore profile boundary. We have selected a magnification which relates to the camera enlargement in order to allow the major pore structure of macroporous polystyrenes with a wide range of densities to be examined in parallel and

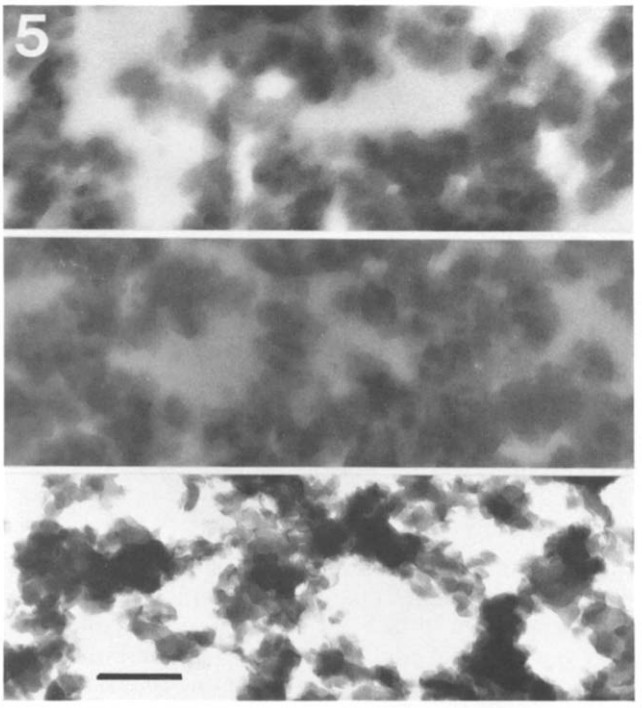

Figure 5 Transmission electron micrographs of sorbent PS20X1ET: top, dry; centre, freeze-dried; bottom, frozen. Bar = 200 nm

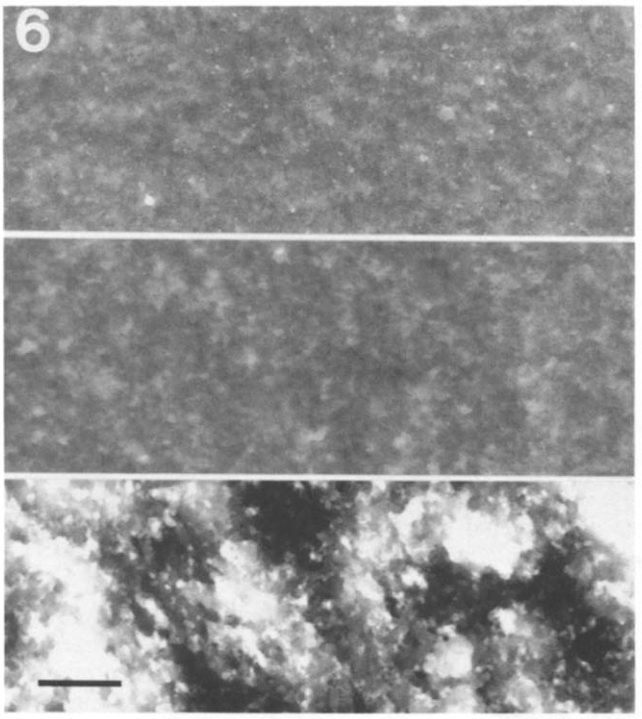

Figure 6 Transmission electron micrographs of sorbent PS55X1T: top, dry; centre, freeze-dried; bottom, frozen. Bar = 200 nm

under identical conditions. We are therefore highly confident about the comparative value of the images we have evaluated.

Effect of crosslink ratio and porogen level on the pore structure of sorbents

The whole matrix of sorbents prepared with toluene as the porogen would be expected to fall within the macroporous domain[7], in view of the high levels of divinylbenzene employed. The micrographs of dry resins (*Figures 1–3*) confirm that this is indeed the case. Visual inspection of these shows a remarkable similarity between the group of sorbents produced with 55 vol% divinylbenzene and those produced with 80 vol%. Within each of these groups it is clear that the average pore profile diameter increases as the proportion of porogen employed is increased. In contrast the group of resins prepared from 100 vol% *p*-divinylbenzene show a progressive decrease in average pore profile diameter with increasing levels of toluene porogen and, superficially at least, sorbent PS100X0.5T appears very similar to PS55X3T and PS80X3T. Likewise PS100X3T looks very similar to PS55X0.5T and PS80X0.5T. These first hand observations are confirmed and quantified below. It is important to remember that the 100X sorbents were prepared from *p*-divinylbenzene, while both the 55X and 80X utilized a mixture of *meta*- and *para*-isomers. It might therefore be argued that this factor alone may have a significant influence. In practice pure divinylbenzene isomers have been used previously to prepare styrene copolymer resins, though generally these have had much lower levels of crosslinker than in the present case[17–20]. While some structural differences have been observed these tend to be rather small, and must be regarded as secondary effects relative to the differences observed here between 55X and 80X sorbents and 100X sorbents. In the former two groups of sorbents the morphology probably evolves according to the model detailed by Guyot[7], i.e. crosslinked nucleii are formed at low conversion and interbonding occurs between these as polymerization continues. As the proportion of solvating porogen employed is increased, the process of interbonding becomes progressively reduced and as a result the final sorbent possesses a larger total pore volume and average pore diameter. In the case of the 100X species, however, the very high divinylbenzene content probably

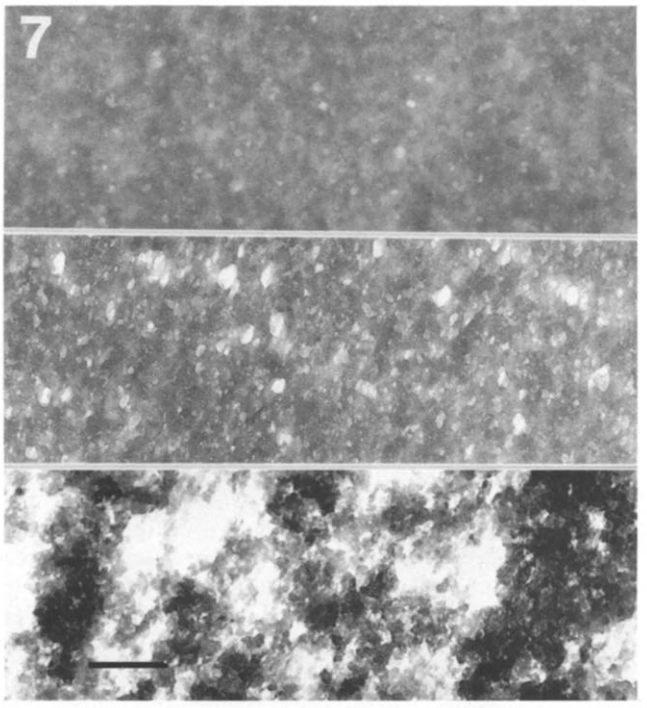

Figure 7 Transmission electron micrographs of sorbent PS100X1T: top, dry; centre, freeze-dried; bottom, frozen. Bar = 200 nm

Table 2 Overall image analysis data for dry, freeze-dried and frozen resin sorbents

Sorbent	Sorbent state	No. of pore profiles examined	Pore profile area		Pore profile diameter	
			Range (nm^2)	Total[a] (μm^2)	Range (nm)	Average (nm)
PS55X0.5T	dry	4834	7–3200	0.0234	3–119	9.4
	freeze-dried	5471	7–10 160	0.0438	3–259	11.1
PS55X1T	dry	8172	7–10 590	0.0691	3–256	11.4
	freeze-dried	7649	7–14 000	0.0708	3–345	11.7
	frozen[b]	2933	7–45 000	0.1469	3–523	24.5
PS55X2T	dry	2224	7–24 160	0.1144	3–336	26.1
	freeze-dried	2060	7–18 940	0.1144	3–318	25.9
PS55X3T	dry	3130	7–12 130	0.1093	3–256	22.3
	freeze-dried	1394	7–108 910	0.1663	3–619	34.9
PS80X0.5T	dry	4418	7–5350	0.0248	3–175	9.9
	freeze-dried	3852	7–5470	0.0288	3–243	11.2
PS80X1T	dry	7305	7–6720	0.0535	3–209	10.4
	freeze-dried	6333	7–10 340	0.0537	3–231	11.8
PS80X2T	dry	3210	7–4090	0.0619	3–134	17.6
	freeze-dried	2693	7–14 360	0.0839	3–252	20.5
PS80X3T	dry	2289	7–25 900	0.1025	3–417	22.7
	freeze-dried	1517	7–46 340	0.1798	3–698	38.2
PS100X0.5T	dry	16 141	7–23 430	0.1206	3–453	23.8
	freeze-dried	3821	7–25 790	0.1787	3–698	35.1
PS100X1T	dry	7272	7–27 480	0.0902	3–373	18.9
	freeze-dried	10 731	7–49 130	0.0774	3–511	13.8
	frozen[b]	4708	7–28 000	0.1287	3–303	20.1
PS100X2T	dry	5766	7–13 160	0.0887	3–266	19.2
	freeze-dried	6263	7–11 720	0.0972	3–236	18.3
PS100X3T	dry	7288	7–15 040	0.0537	3–260	15.5
	freeze-dried	5897	7–9458	0.0631	3–169	17.5
PS20X1ET	dry	539	7–165 000	0.2444	3–979	67.4
	freeze-dried	629	7–180 000	0.2012	3–975	50.9
	frozen[b]	681	7–222 000	0.3888	3–942	63.9

[a]For a total image area of 1 μm^2
[b]Nominal sample thickness increased to ~80 nm (see Experimental)

gives rise to the very rapid generation of a highly rigid, strained and dense matrix of crosslinked polymer chains at low conversion, which in the case of the lowest level of porogen quickly 'locks in' a well-defined pore structure. Indeed, the situation probably corresponds quite closely to that when a precipitating porogen is used[21]. As the proportion of toluene porogen is increased, the whole process of pore formation is probably increasingly delayed by the more extensive solvation of the macromolecular matrix. This allows some equilibration in the morphology and a more uniform evolution of nucleii and syneresis of porogen, resulting in smaller pore formation. The situation with higher porogen levels in effect is much closer to the model detailed by Guyot[7].

Image analysis data of dry resins

Overall data for dry and freeze-dried sorbents are shown in *Table 2*, where the numbers of pore profiles examined are also shown. It is believed that these are more than sufficient for the data to be statistically significant. The results from the dry resins confirm the visual observations made above. Histograms of the total pore cross-sectional areas (μm^2 per 1 μm^2 of examined area) (*Figure 8*), and average pore profile diameters (*Figure 9*) show the observed trends more clearly, again highlighting the difference between the 100X group and the 55X and 80X groups. Irrespective of the level of crosslinker (55–100X) used in a sorbent it seems that the maximum pore profile cross-sectional area, A, achievable per 1 μm^2 of sorbent area is very similar, ~0.12 μm^2, i.e. about one-eighth. This is obtained with a toluene porogen level of 3/1 (v/v) relative to monomer in the case of the 55X and 80X series, but with only 0.5/1 (v/v) in the case of the 100X group. Similarly the upper limit to the average pore profile diameter, d, is also very similar in the three series of sorbents, ~22 nm. These results agree with data from other physical measurements (N_2 sorption/desorption, Hg intrusion porosimetry) on structurally similar polymers[6]. It seems that significant deviations from these limiting parameters can be achieved only by employing precipitating (and polymeric[7])

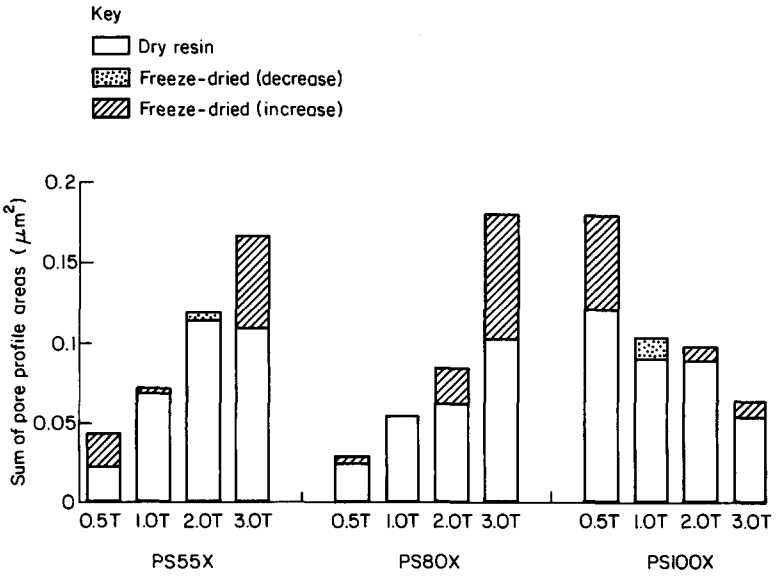

Figure 8 Differences in total pore profile cross-sectional areas, A, between dry and freeze-dried samples of resin sorbents

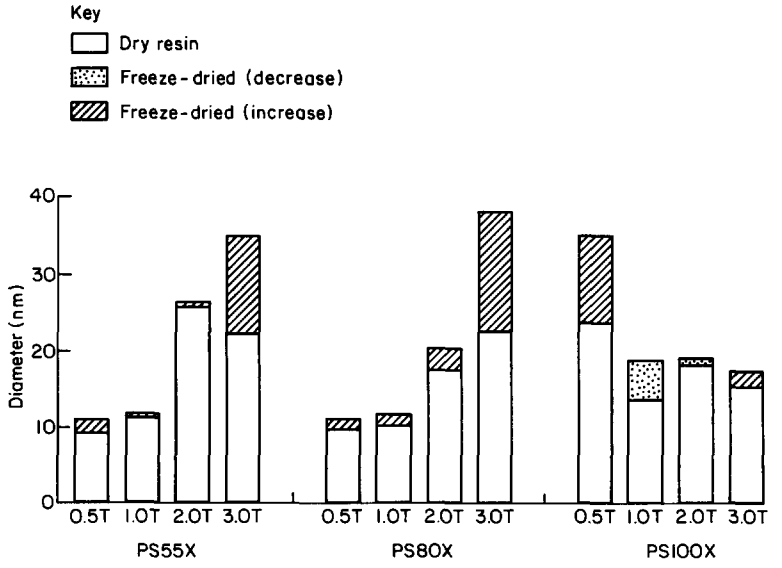

Figure 9 Differences in average pore profile diameters, d, between dry and freeze-dried samples of resin sorbents

porogens, and the data for dry PS20X1ET confirm this (*Table 2*). The total pore profile cross-sectional area for this sorbent is $\sim 0.24\ \mu m^2$ per $1\ \mu m^2$ of examined area, and the average pore profile diameter is ~ 68 nm. Again this data is consistent with earlier data from other physical measurements on similar dry resins and adds considerably to the validity of our techniques.

Effects of hydration: freeze-dried samples

Micrographs of some of the freeze-dried and frozen samples are shown in *Figures 5–7*, and the corresponding image analysis data for all the samples examined are summarized in *Table 2*. The effects of hydration are indeed manifest. In most cases, the freeze-dried samples show an increase in both the total pore profile cross-sectional area and the average pore profile diameter. The changes are seen most clearly in the histograms in *Figures 8* and *9* which show that the increases tend to be largest for the dry resins with the largest average pore profile diameters, i.e. PS55X3T, PS80X3T and PS100X0.5T. In some instances small contractions are seen. Overall these results confirm that hydrophobic sorbents based upon styrene–divinylbenzene do undergo very significant porosity changes when hydrated. While no major macroscopic swelling of sorbent beads is readily observed in water, quite clearly hydration allows considerable internal adjustment to the morphology, probably via plasticization of polymer chains and, in particular, the relief of steric strain. This is probably closely related to the reported effects of water on hypercrosslinked resins[22].

The observation and quantification of these hydration changes also explain why it has been very difficult to correlate porosity characteristics (from conventional methods) of dry sorbents with, for example, sorption performance. Before it is possible to do this with any

Table 3 Proportion of total pore profile cross-sectional area associated with specific ranges of pore profile diameters

Sorbent	Sorbent state	Pore profile cross-sectional area (%) within pore diameter ranges (nm)					
		<8	8–11	11–25	25–50	50–80	>80
PS55X0.5T	dry	24.5	12.7	40.2	18.1	4.5	0
	freeze-dried	14.4	5.4	24.8	30.2	15.2	9.9
PS55X1T	dry	13.3	6.2	30.2	29.9	10.6	9.8
	freeze-dried	11.8	6.5	28.4	33.9	13.8	5.6
PS55X2T	dry	1.4	0.8	8.3	30.3	29.9	29.3
	freeze-dried	1.3	1.1	10.3	23.4	25.1	38.8
PS55X3T	dry	2.4	2.3	15.9	37.8	28.8	12.6
	freeze-dried	0.6	0.4	3.6	11.8	16.7	66.7
PS80X0.5T	dry	20.9	10.6	38.9	20.1	3.2	6.3
	freeze-dried	14.8	8.3	38.5	32.1	4.3	1.8
PS80X1T	dry	15.6	6.3	26.1	31.9	15.4	4.7
	freeze-dried	14.8	8.3	38.5	32.1	4.3	1.8
PS80X2T	dry	4.0	5.4	36.2	43.5	10.6	0
	freeze-dried	2.5	2.5	17.8	38.8	25.7	12.7
PS80X3T	dry	2.1	1.4	11.1	29.8	29.1	26.5
	freeze-dried	0.9	1.2	10.6	28.1	28.3	30.9
PS100X0.5T	dry	1.4	1.4	13.8	23.5	20.6	27.2
	freeze-dried	0.5	0.6	4.3	12.9	20.1	61.6
PS100X1T	dry	2.4	1.7	13.8	29.9	24.4	27.8
	freeze-dried	6.3	4.5	25.5	28.5	15.1	20.1
PS100X2T	dry	2.6	2.6	14.2	32.2	32.8	15.6
	freeze-dried	3.8	3.8	27.4	37.6	14.8	12.8
PS100X3T	dry	4.8	4.4	28.2	32.6	15.5	14.5
	freeze-dried	3.0	2.8	21.4	37.4	25.5	9.9

Table 4 Pore[a] profile circularity[b] and shape[c]

Sorbent	Sorbent state	Pore circularity	Pore shape
PS55X0.5T	dry	0.93	0.47
	freeze-dried	0.90	0.44
PS55X1T	dry	0.89	0.54
	freeze-dried	0.90	0.46
PS55X2T	dry	0.83	0.51
	freeze-dried	0.84	0.52
PS55X3T	dry	0.85	0.51
	freeze-dried	0.82	0.51
PS580X0.5T	dry	0.92	0.46
	freeze-dried	0.90	0.48
PS80X1T	dry	0.91	0.43
	freeze-dried	0.90	0.49
PS80X2T	dry	0.90	0.56
	freeze-dried	0.85	0.53
PS80X3T	dry	0.84	0.50
	freeze-dried	0.87	0.56
PS100X0.5T	dry	0.79	0.56
	freeze-dried	0.74	0.55
PS100X1T	dry	0.79	0.53
	freeze-dried	0.81	0.52
PS100X2T	dry	0.78	0.53
	freeze-dried	0.88	0.54
PS100X3T	dry	0.79	0.53
	freeze-dried	0.79	0.55

[a] Pores > 8 nm
[b] $4\pi A/p^2$ (circle = 1)
[c] A/dw (see *Figure 4*)

great reliability, more detailed information on the hydrated state of sorbents is required and the present work has shown how this can be achieved.

Tables 3 and *4* show more detailed breakdowns of the image analysis data. The observed increases in average pore profile diameters of dry resins on hydration are clearly seen to arise from a shift in the whole pore size distribution towards larger pores (*Table 3*). The effect is particularly marked with PS55X3T, PS80X3T and PS100X0.5T. The data can also be manipulated further, for example, to quantify the change in distribution of pore profile cross-sectional area on hydration as a function of pore profile diameter. This is potentially important because the contribution from some pore sizes decreases while that of others increases, and such data may in due course be of value in tailoring sorbents for particular applications. In this instance we illustrate the possibilities with a histogram for sorbent PS55X0.5T (*Figure 10*) which shows that the cross-over point above which pore profile area increases, and below which it decreases on hydration, is ~55 nm. The corresponding values for PS80X2T and PS100X0.5T, for example, are ~65 nm and ~130 nm.

Symmetry of pores

Table 4 shows the changes in the symmetry of pore profiles in terms of their circularity and shape. For dry

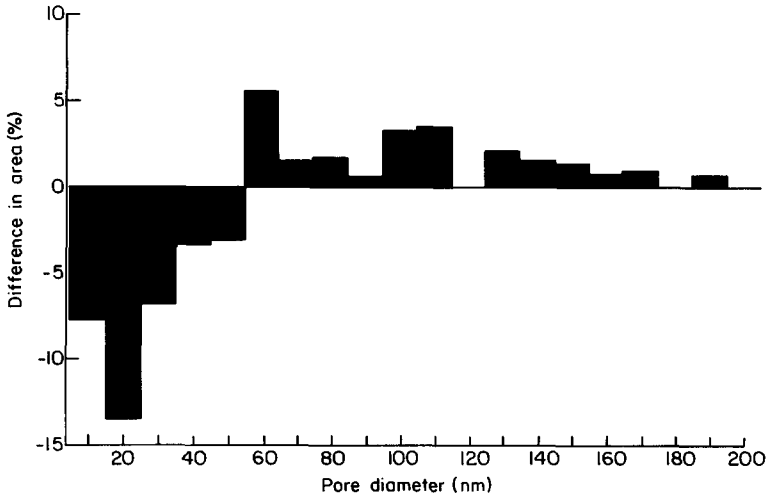

Figure 10 Change in pore profile cross-sectional area as a function of pore diameter in moving from dry to freeze-dried PS55X0.5T

resins the circularity falls progressively as the crosslink ratio employed increases from 55 to 100%. Within the 55X and 80X groups the circularity also falls as the proportion of porogen employed is increased. However, the reverse trend is seen in the 100X series, again emphasizing the structural difference of this group. The effect of hydration on pore symmetry is more varied. In the case of sorbents prepared with low levels of porogen (0.5T) circularity falls on hydration. In all cases measurable changes are observed, even in those resins where the difference between values for the total pore profile area between dry and freeze-dried species is only slight, e.g. PS80X1T. This tends to confirm that subtle hydration effects arise even when major changes in pore dimensions are not apparent.

Image analysis data of frozen sorbents

Because of the difficulty in obtaining satisfactory thin sections from frozen hydrated sorbents, much less quantitative data is available for these species (limited to PS55X1T, PS100X1T and PS20X1ET, *Table 2*). Because slightly thicker sections were required for mounting and imaging, quantitative comparison with the data for dry and freeze-dried samples should not be pushed too far. In addition, whilst polystyrene is remarkably resistant to beam damage compared to other organic polymers and biological material containing light elements, specimen damage to polymer sections unprotected by an embedding medium and heavy metal stains could induce significant quantitative changes to the matrix structure, and thus adversely affect an analysis of binary images. With the pore space being filled with water rather than Lowicryl resin during sectioning, frozen sections have an apparently much greater contrast between the polymer matrix and its pore void. This alone partly explains the seemingly 'lumpy' texture of the matrix. In addition, the natural holes which represent the pore space increase the local susceptibility of the matrix to beam damage at its edge, thus potentially artificially enlarging the pore void during examination and again possibly contributing to the lumpy appearance. A more definitive approach to analysis in follow-up work might be to examine frozen hydrated polymer at low temperature, e.g. $-150°C$, using a cold stage, and then to assess the changes following freeze-drying *in situ*. Even bearing these factors in mind, however, it is quite clear from the data that additional significant changes in pore structure are observed in the case of the frozen samples. With PS55X1T and PS100X1T the total pore profile areas are more or less double those from the dry state, with a correspondingly large increase in the average pore profile diameters. In contrast the changes for PS20X1ET, prepared with a precipitating porogen, are much less, suggesting that the data are indeed not artificial. PS20X1ET, a precipitated resin with relatively large pore diameters, would be expected to be a more rigid and entangled network than the others, prepared with a solvating porogen, and the relatively minor changes seen in the pore structure of PS20X1ET on hydration tends to confirm this.

It does seem, therefore, that the changes observed with the frozen hydrated samples are likely to be a better representation of the hydrated state of the sorbents than the changes seen with freeze-dried sections. Possibly the latter shrink whilst drying at $-70°C$ and/or during infiltration of the precured Lowicryl embedding resin. The data obtained from freeze-dried sections probably represent the minimum changes which occur on hydration of sorbents, and in reality 'wet' samples are even more swollen than these data imply. In terms of analysing and quantifying swelling, however, the freeze-drying and embedding procedure is a more robust and reproducible method and is certainly much easier to perform than the sectioning of frozen hydrated samples.

CONCLUSIONS

(1) It is possible to use energy filtered TEM (no heavy metal staining of sample sections) to produce real images of polymer sections.
(2) Image analysis techniques can be applied to evaluate the pore structure of polymers quantitatively.
(3) Such analysis has shown that hydrated hydrophobic porous polymers do swell significantly relative to their dry state and the changes in pore structure have been qualified.
(4) Use of freeze-dried samples is experimentally more straightforward and the data from such samples

more reproducible than is the case with hydrated frozen sections.

(5) This approach is likely to be much more widely applicable to other porous systems whether they be inorganic[23] or organic-based, from a natural or synthetic source.

(6) Such data will be of value to those technologists designing polymeric sorbents for particular applications.

ACKNOWLEDGEMENTS

We acknowledge with thanks the receipt of a post-graduate research fellowship for B.R. and a post-doctoral research fellowship for I.M.H. from the UK Science and Engineering Research Council. We are also grateful to the Dow Chemical Co. for the gift of the 80 vol% divinylbenzene. Finally, we thank Margaret Mullin for technical support, and Peter Rickus for photographic expertise.

REFERENCES

1 Dorfner, K. (Ed.) 'Ion Exchangers', Walter de Gruyter, Berlin, 1991
2 Millar, J. R. *J. Polym. Sci. Polym. Symp.* 1980, **68**, 167
3 Simpson, R. M. 'The Separation of Organic Chemicals from Water', presented at the 3rd Symposium of the Institute of Advanced Sanitation Research, April 1972 (reprint available from Rohm and Haas, Philadelphia, PA 19105, USA)
4 Voser, W. *J. Chem. Technol. Biotechnol.* 1982, **32**, 109
5 Pirotta, M. *Angew. Makromol. Chem.* 1982, **109/110**, 197
6 Albright, R. L. *Reactive Polym.* 1986, **4**, 155
7 Guyot, A. in 'Syntheses and Separations Using Functional Polymers' (Eds D. C. Sherrington and P. Hodge), J. Wiley, Chichester, 1988, Ch. 1, p. 1
8 Rowatt, B. and Sherrington, D. C. 'Proc. IEX '92', SCI, in press
9 Millar, J. R., Smith, D. G., Marr, W. E. and Kressman, T. R. E. *J. Chem. Soc.* 1963, 218
10 Spontak, R. J., Williams, M. C. and Schoolay, C. N. *J. Mater. Sci.* 1986, **21**, 3173
11 Huxham, I. M., Rowatt, B., Tetley, L. and Sherrington, D. C. *Trans. R. Microsc. Soc.* 1990, **1**, 207
12 Robards, A. W. and Sleyta, U. B. in 'Low Temperature Methods in Biological Electron Microscopy', Vol. 10 of 'Practical Methods in Electron Microscopy' (Ed. A. M. Glauert), Elsevier, Amsterdam, 1985
13 Echlin, P., Ralph, B. and Weibel, E. R. (Eds), 'Low Temperature Biological Microscopy and Microanalysis', Reprints of *J. Microsc.*, Vols 110–112, The Microscopical Society, Oxford, 1978
14 Lindsay, D. and Sherrington, D. C. *Reactive Polym.* 1985, **3**, 327
15 Huxham, I. M., Rowatt, B., Tetley, L. and Sherrington, D. C. *J. Microsc.* 1991, **162**, 191
16 Rowatt, B., Huxham, I. M., Tetley, L. and Sherrington, D. C. in preparation
17 Wiley, R. H., Kim, K. S. and Rao, S. P. *J. Polym. Sci. Part A1* 1971, **9**, 805
18 Wiley, R. H. and Kim, K. S. *J. Macromol. Sci. Chem.* 1974, **A8**, 687
19 Schwachula, G. *J. Polym. Sci. Polym. Symp.* 1975, **53**, 107
20 Schwachula, G. *Zeit. Chemie* 1978, **18**, 242
21 Kun, K. A. and Kunin, R. *J. Polym. Sci. Part A1* 1968, **7**, 2689
22 Davankov, V. A. and Tsyurupa, M. P. *Reactive Polym.* 1990, **13**, 27
23 Kerch, H. M., Gerhardt, R. A. and Grazul, J. L. *J. Am. Ceram. Soc.* 1990, **73**, 2228